Karimi, N., Ng, K. T. W., Richter, A., Williams, J., & Ibrahim, H. (2021). Thermal heterogeneity in the proximity of municipal solid waste landfills on forest and agricultural lands. *Journal of Environmental Management*, 287, 112320-. https://doi.org/10.1016/j.jenvman.2021.112320

Thermal Heterogeneity in the Proximity of Municipal Solid Waste Landfills on Forest and Agricultural Lands

Full Length Article

Nima Karimi [a], Kelvin Tsun Wai Ng [a], Amy Richter [a], Jason Williams [b], Hussameldin Ibrahim [b]

[a] Environmental Systems Engineering, Faculty of Engineering and Applied Science, University of Regina, 3737 Wascana Parkway, Regina, SK, S4S 0A2, Canada.
[b] Clean Energy Technologies Research Institute, Process Systems Engineering, Faculty of Engineering and Applied Science, University of Regina, 3737 Wascana Parkway, Regina, SK, S4S 0A2, Canada.

Corresponding author:

Kelvin Tsun Wai Ng, PhD, P.Eng
Environmental Systems Engineering
University of Regina, 3737 Wascana Parkway
Saskatchewan, Canada S4S 0A2
ORCID: 0000-0002-2045-9367
Email: kelvin.ng@uregina.ca
Phone: (306) 337-8487 | Fax: (306) 585-4855

Declarations of interest: none.

Abstract:

Information on the spatial extent of potential impact areas near disposal sites is vital to the development of a sustainable natural resource management policy. Eight Canadian landfills of various sizes and shapes in different climatic conditions are studied to quantify the spatial extent of their bio-thermal zone. Land surface temperature (LST) and normalized difference vegetation index (NDVI) are examined with respect to different Land Use Land Cover (LULC) classes. Within 1500 m of the sites, LST ranged from 18.3 °C to 29.5 °C and 21.3 °C to 29.7 °C for forest land and agricultural land, respectively. Linear regression shows a decreasing LST trend in forest land for five out of seven landfills. A similar trend, however, is not observed for agricultural land. Both the magnitude and the variability of LST are higher in agricultural land. The size of the bio-thermal zone is sensitive to the respective LULC class. The approximate bio-thermal zones for forest class and agricultural classes are about 170 ± 90 m and 180 ± 90 m from the landfill perimeter, respectively. For the forest class, NDVI was negatively correlated with LST at six out of seven Canadian landfills, and stronger relationships are observed in the agricultural class. NDVI data has a considerably larger spread and is less consistent than LST. LST data appears more appropriate for identifying landfill bio-thermal zones. A subtle difference in LST is observed among six LULC classes, averaging from 23.9 °C to 27.4 °C. Geometric shape makes no observable difference in LST in this study; however, larger landfill footprint appears to have higher LST.

Keywords: Solid waste management; municipal landfill design and regulations; land surface temperature; normalized difference vegetation index; bio-thermal zone; land use and land cover

1 Introduction

Landfilling and open dumping of waste is one of the most commonly used solid waste treatment processes across the globe (IPCC, 2019). Lack of technical knowledge and financial resources in developing countries often results in poorly managed land disposal sites (Bellezoni et al. 2014; Karimi et al. 2019). In addition, proper identification and monitoring of open dumps are difficult due to their secretive nature and the sheer number of sites, as well as rapid population growth and urbanization (Sharma et al. 2018). The United Nation's Intergovernmental Panel on Climate Change (IPCC) reports that waste disposal is an important contributor of greenhouse gases such as carbon dioxide, methane, and nitrogen oxides, accounting for about five percent of total global greenhouse gas generation (IPCC, 2019). Leachate generated from anaerobic decomposition of waste has also been linked to soil and groundwater contamination which impacts proximal human and plant health (Xu et al. 2018).

Effects of land cover changes on land surface temperature (LST) have been well documented in a number of studies (Ramachandra et al. 2018; Ullah et al. 2019; Yang et al. 2020). Specifically, studies have reported that open dump sites have negatively impacted vegetation growth due to the soil degradation resulting from site operation (Basso et al. 2004; Mahmood et al. 2016). Compared to modern landfills, open dump sites have minimum containment measures regarding mass and heat flux, but are typically smaller in size. According to Phil-Eze (2010), disposal and degradation of municipal waste can alter soil chemistry and irreversibly impact nearby plant species structure and fertility. A Nigerian study focused on soil metal concentration near dump sites and found elevated metal concentrations in the first 40-centimeter depth of the soil (Azeez et al. 2011). A field study in Pakistan confirmed that tangible subterranean destructive changes such as lower metabolism rate and lower diversity in plant species occur in the vicinity of dump sites (Ali et al.

2014). In addition to the direct environmental impacts associated with landfill gas and leachate generation, heat generated by the waste biological decomposition, metal corrosion, and ash hydration/carbonation at landfill site may be significant (Hao et al, 2017). Excessive heat originating from decomposition of organics are recorded and documented in multiple landfills (Koerner and Koerner 2006). Elevated land surface temperature is also reported in a number of landfill sites in the USA and Canada (Hanson et al. 2009), and in China (Cai et al. 2014). The heat accumulation in landfills may impact microclimate and nearby vegetation health.

Recently, Mahmood et al. (2017) used remote sensing techniques to detect distressed vegetation zones near open dumps located in semi-arid regions and reported increases in surface temperature together with decreases in various remote sensing vegetation indexes. It appears that disposal site operation may impact microclimatic condition, and monitoring vegetation health level using remote sensing techniques may be an indirect and affordable way to assess and delineate polluted areas (Mahmood et al. 2019).

Most landfill studies focus on the impact of leachate on groundwater quality (Xu et al. 2018, Pan et al. 2019b) and modelling of landfill gas and fugitive emissions (Bruce et al. 2018; Mønster et al. 2019). However, the extent and severity of the bio-thermal zone of modern landfills (with engineered liner, leachate collection system, cover, and gas management system) have been mostly neglected in the literature, perhaps giving a false sense of security regarding their environmental performance. Yan et al. (2014) analyzed two engineered landfills in Ottawa, Canada, with Landsat satellite imagery and found that land surface temperature at modern landfills are higher than nearby vegetated areas as well as ambient temperature. In countries with a heavy reliance on landfilling as their primary waste treatment method, quantification of the spatial extent of vegetative distress zone is important and may help to develop strategies to mitigate these effects. This is increasingly

important, as physical distance between landfills and population centers has been decreasing due to urbanization and population growth.

Canadians send most of their municipal waste to landfills for permanent disposal (Chowdhury et al. 2017, Pan et al. 2019a, Richter et al., 2018). In 2016, Canadians generated 943 kg per capita, with a waste diversion rate of about 27% (Statistics Canada, 2019). In this study, eight engineered landfills in Canada with various size and shape are selected and systematically studied to quantify the spatial extent of the bio-thermal zone using satellite imagery. The objectives of this study are to [i] identify probable bio-thermal zones in the vicinity of engineered landfills by tracking land surface temperature (LST) and vegetation health anomalies using normalized difference vegetation index (NDVI) with respect to the land use and land cover (LULC) classification, in different climatic conditions; and [ii] examine the rate of changes of the selected indicators within and beyond the bio-thermal zone.

Table 1 shows an overview of major studies that combine remote sensing imagery and classification for landfill site detection and monitoring purposes. Most studies used satellite imagery to determine the attributes of the inner part of the landfills, regardless of what is happening in the vicinity of landfills. For example, Hanson et al. (2009) analyzed the temperature of four North American landfills and observed a gradual increase in temperature with respect to warmer climatic regions of landfills. Iacoboaea and Petrescu (2013) applied Landsat multi-temporal imagery to monitor temperature changes within their landfill and showed that Landsat imagery could be used as a supportive dataset for monitoring and detection purposes. The novelty of this study is that it explicitly considers the effects of the bio-thermal zone near modern landfills on multiple LULC classes (Table 1). Unlike other studies using satellite imagery to study the bio-thermal effect of disposal sites, this study explicitly considers the effects of land use, geometric

shape, and spatial footprint of the waste sites. Urbanization and lack of suitable landfill sites in cities (Garkowski and Hostovsky, 2011) have generated a need for more stringent knowledge of land information for sustainable natural resource management and better wildlife habitat protection. The spatial extent of potential impact areas near modern landfills is vital to the development of necessary mitigation and remediation actions.

125

126 Table 1- Recent literature applying remote sensing imagery to identify and monitor landfill disposal site features and adverse effects in
127 surrounding areas
128

Reference	Type of remote sensing data or ground measurement	Number of disposal sites investigated	Type of disposal site & total footprint of disposal sites, in km^2	Use of surface temperature in detecting anomalies (bio-thermal zone)	Use of vegetation health indices in detecting anomalies (bio-thermal zone)	Separate classes and data analysis in individual classes	Number of classes used in classification system	Study area
Hanson et al. (2009)	Ground measurements	4	Landfill; 0.65 - 2.25	✓	-	-	-	Alaska, British Columbia, Michigan, and New Mexico
Biotto et al. (2009)	IKONOS satellite data	54	Landfill; area not available	-	-	✓	-	North-east Italy
Shaker et al. (2010)	Landsat TM and ETM sensors	-	Landfill; area not available	✓	-	-	-	Jeleeb Al-Shuyoukh area, Kuwait
Iacoboaea and Petrescu (2013)	Landsat4 TM, Landsat5 TM and Landsat7 ETM+	1	Landfill; 1.20	✓	-	-	-	Glina, Romania
Yan et al. (2014)	Landsat 4,5 TM	2	Landfill, area not available	✓	✓	-	-	Ottawa, Canada
Mahmood et al. (2017)	Landsat 8 OLI and TIRS	2	Open dump; 0.14 - 0.28	✓	✓	-	3	Lahore, Pakistan
Mahmood et al. (2019)	Landsat 8 imagery from 2013 to 2015	2	Open dump; 0.14 - 0.28	-	✓	-	-	Lahore, Faisalabad, Pakistan
Current Study	Landsat 8 OLI and TIRS	8	Landfill; 0.06 to 1.84	✓	✓	✓	6	Western, central (prairies), and eastern Canada

129

130

131

132

133

2 Methodology

2-1 Landfill site selection

Eight Canadian landfills with various footprints (0.06 million m^2 to 1.8 million m^2) and geometric shapes (rectangular to rounded) are selected, as shown in Figure 1. All selected landfills have published annual reports in the public domain, detailing disposal rate, and leachate and gas management systems. The selected sites are located in three Canadian provinces (British Columbia, Saskatchewan, and Ontario) with different climatic conditions to examine the characteristics of bio-thermal zone.

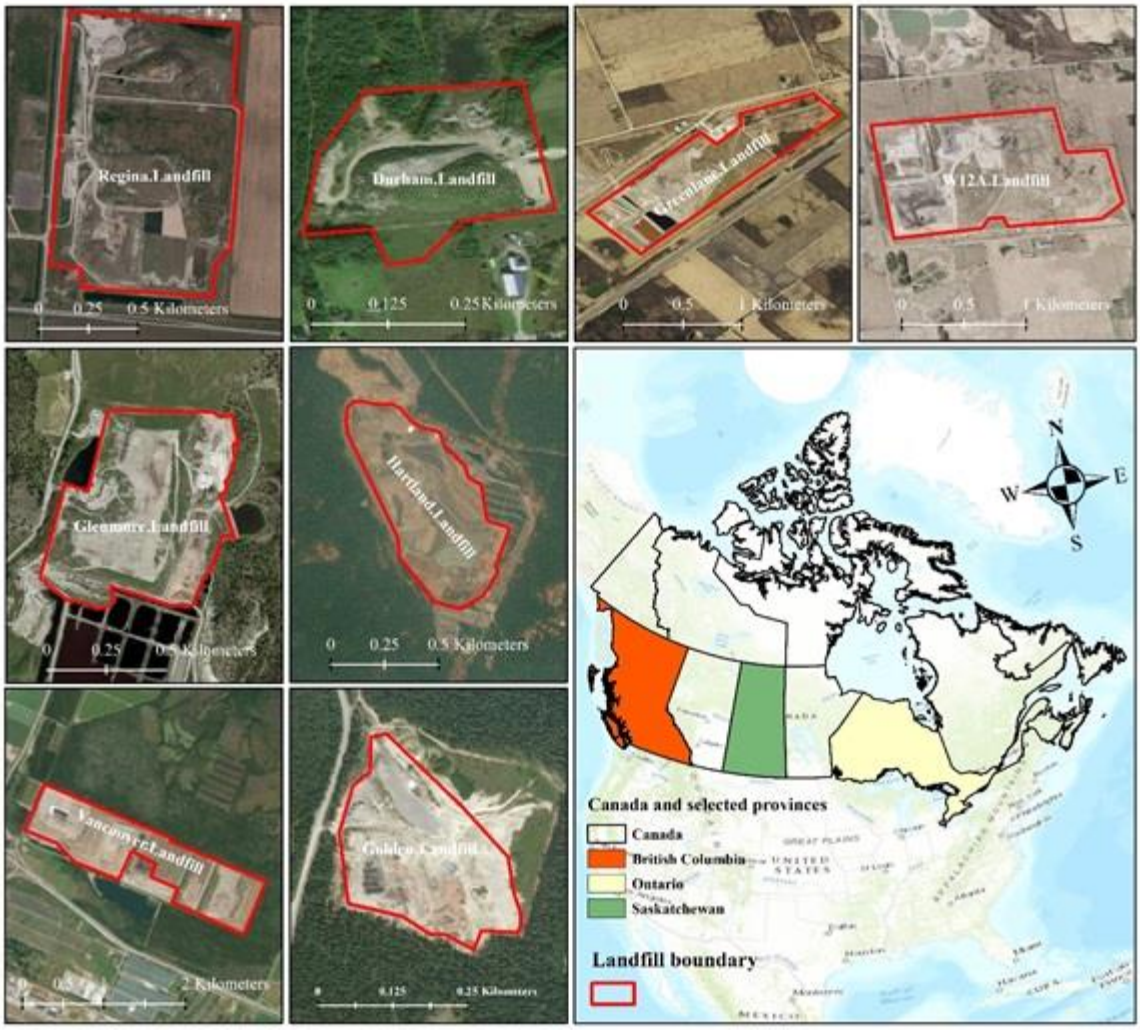

Figure 1-Spatial footprint and geometric shape of the eight Canadian landfills

Landfill leachate, gas, and heat are by-products of the anaerobic digestion of the organic fraction of waste organic. Table 2 summarizes the key parameters that may affect the size of bio-thermal zone. Six of the studied landfills have active leachate collection systems, and seven have landfill gas management systems. Landfill site characteristics such as geometric shape, site perimeter, and area are reported in Table 3.

151

152 Table 2 – Locations and specifications for eight Canadian Landfills

Landfill	Location (Decimal degree) Latitude/Longitude	Leachate management system	Gas management system
Golden (Golden 2017)	51.308854°/ -116.951570°	With an active leachate collection system or similar leachate management system.	Does not have a gas management system. Gas monitoring probes are installed.
Greenlane, Toronto (City of Toronto 2017)	42.813247°/ -81.326794°	Has an active leachate collection system or similar leachate management system.	Has an active gas management system. Landfill gas collection and flaring system is in normal operation at the time of study.
Durham (Annual monitoring report 2017)	44.167302°/ -80.828247°	Does not have an active leachate collection system. Monitoring the observation wells show the concentrations of leachate indicator parameters below the criteria of MOECC (Ministry of Environment) guidelines.	Has an active gas management system. Methane gas concentration is within acceptable range.
Glenmore (Glenmore landfill 2017)	49.958464°/ -119.417680°	Has an active leachate collection system or similar leachate management system.	Has an active gas management system.
Hartland (Hartland Landfill 2016)	48.536959°/ -123.463997°	Has an active leachate collection system or similar leachate management system.	Has an active gas management system commissioned in 2016
Vancouver (Vancouver Landfill 2017)	49.101781°/ -123.004492°	Has an active leachate collection system or similar leachate management system. The 2017 monitoring program met or exceeded the regulatory requirements.	Has an active gas management system. Both vertical and horizontal pipes are used.
W12A (W12A Annual Report 2017)	42.879615°/ -81.229547°	Does not have an active leachate collection system.	Has an active gas management system. The collected gas is flared to control the methane concentration to an acceptable level.
Regina (City of Regina 2009)	50.491619°/ -104.543224°	Has an active leachate collection system or similar leachate management system.	Has an active gas management system. The collected gas is flared to control the methane concentration to an acceptable level.

153

154

155

Table 3 - Date of satellite image acquisition, association between forest/agricultural land and LST as Pearson correlation coefficient, and geometric features for eight Canadian landfills

Landfill ID/ Source	Footprint approximate geometric shape	Satellite acquired image date YYYY.MM.DD	Pearson correlation coefficient between LST and NDVI ($p < 0.05$)		Estimated site perimeter (m)	Estimated site area (m^2)
			Forest	Agricultural		
Vancouver (Vancouver Landfill 2017)	Elongated	2018.08.09	-0.30	-0.79	7,819	1,841,113
Hartland (Hartland Landfill 2016)	Rounded	2018.07.24	-0.69	N/A	2,681	386,883
Greenlane, Toronto (City of Toronto 2017)	Elongated	2018.08.14	-0.69	-0.92	4,341	715,965
W12A (W12A Annual Report 2017)	Rectangular	2018.07.04	-0.38	-0.44	4,564	1,129,820
Golden (Golden 2017)	Rounded	2018.06.17	-0.18	N/A	1,060	64,486
Glenmore (Glenmore landfill 2017)	Rectangular	2018.08.27	+0.35	-0.53	3,143	503,319
Durham (Annual monitoring report 2017)	Rounded	2018.06.02	-0.50	-0.71	1,010	59,233
Regina (City of Regina 2009)	Rectangular	2018.08.12	N/A	-0.97	4,527	1,182,427
AVERAGE					3,643	735,406

Note: N/A = not available. Footprint approximate geometric shapes are visually determined from Figure 1. Pearson correlation coefficient results are discussed in Section 3.3.

2-2-Landsat 8 Imagery

The Landsat 8 Operational Land Image and Thermal Infrared Sensory (OLI/TIRS) instrument has 11 bands ranging from 0.43 up to 12.51 µm, and covers all visible bands. The spatial resolution of bands 1-7 and 9 is 30×30-meter, while band 8 (panchromatic band) has the highest spatial resolution of 15×15-meter. TIRS bands have the lowest spatial resolution of 100×100-meter, however they are delivered in 30×30-meter pixels by USGS to provide a more uniform imagery compare to other bands (USGS, 2020).

TIRS bands are widely used to acquire land surface temperature (Cristóbal et al., 2018; Nikam et al., 2016; Yu et al., 2014). In the current study, Landsat 8 TIRS level 1 imagery was collected in the summer of 2018 to estimate the LST. According to Shaker et al. (2010) and Yan et al. (2014), imagery in warmer seasons provides deeper contrasts of LST in immediate surrounding vegetation and assists in the delineation of hot spots. As such, cloud-free images of the selected landfills and neighboring areas during the summer of 2018 (June, July, and August) are selected (Table 3).

2-3-Landfill borders and buffer rings

Preliminary results suggest that the potential bio-thermal impact of landfills and the spatial distribution of the vegetation stress zone are sensitive to disposal footprint and landfill boundaries. As such, well-defined and precise landfill borders are of great importance. A closer look at the landfill annual reports (Table 2), however, reveals that landfill borders are loosely defined in most cases due to inconsistent definitions. For example, Supplementary Figure 1a depicts all phases of the Vancouver landfill including closed, active, and future disposal areas (Vancouver landfill,

2017). To obtain more precise boundaries of the sites at the time of study, all boundaries are visually inspected and carefully verified using satellite images during the time period. Supplementary Figure 1b shows the final boundary used for the Vancouver landfill in the present study. Using ArcMap (v.10.5), multiple 30-m buffer rings are constructed digitally from the chosen landfill boundary to a distance of 1,500 m. Mahmood et al. (2017) used a similar approach to monitor adverse effects for open dumps in Pakistan. The 30-meter increment is selected due to the maximum spatial resolution of Landsat imagery. Mahmood et al. (2017) found that a major radial effect is observed within 1,000 meters of their 14 and 28 ha non-regulated open dumps. However, in the current study, larger total buffer areas are considered (1,500-meter buffer) for the eight engineered landfill sites in Canada (Figure 1).

LST is computed using the Landsat data as a supporting indicator on the bioactivity of waste decomposition at the eight landfills. Image calibration (conversion from DN values to radiance) and atmospheric correction (conversion from top of atmosphere to bottom of atmosphere reflectance) of the level 1 imagery were performed using Equations 1 and 2, respectively. Equations 3 to 8 are empirical equations to determine the LST provided in the Landsat 8 Data users handbook (Version 4). A web-based atmospheric correction model (Barsi et al. 2003; Barsi et al. 2005) was used to convert TOA to at surface radiance. The spectral radiance (L_λ) can be estimated using Equation 1:

$$L_\lambda = M_L \times Q_{Cal} + A_L \quad (1)$$

L_λ= spectral radiance (watts/m^2×sr×µm)
M_L=Band-specific multiplicative rescaling factor for the band (RADIANCE_MULT_BAND_n)
A_L=Radiance additive scaling factor for the band (RADIANCE_ADD_BAND_n)
Q_{cal}=Level 1-pixel value in DN

Calculated radiance then used as an input to provide the atmospherically corrected radiance (L_T) using Equation 2.

$$L_T = \frac{L_{\lambda - L_{up}}}{\tau \times e} - \frac{1-e}{e} \times L_d \quad (2)$$

Where L_{up}, L_d, τ and e are upwelling radiance, downwelling radiance, atmospheric transmission, and emissivity, respectively. MODTRAN radiative transfer code is used to estimate the first three parameters. This code is available online (NASA, 2019). Input variables for this code are the coordinate system of the downloaded scene and exact acquisition time and date. Emissivity (e) is calculated from Equation (6). Temperature in kelvin (BT) is estimated using Equation 3 (Chander and Markham 2003):

$$BT = \frac{K_2}{\ln\left(\frac{K_1}{L_T} + 1\right)} \quad (3)$$

*w*here:

L_T=Atmospherically corrected spectral radiance (Watts/(m^2× srad × μm))

K_1=First thermal band conversion constant

K_2=Second thermal band conversion constant

To convert BT to LST, NDVI is calculated using Equation 4 (Silleos et al. 2006; USGS, 2018). Since NDVI comes from surface reflectance, reflectance from top of atmosphere has to be corrected. On the other hand, since it is a normalized index that comes from two adjacent bands, negligible differences are estimated comparing the NDVI values from top of atmosphere and surface (Sobrino et al., 2004). Therefore, NDVI is calculated without any correction.

PV, e, and LST are calculated using Equations 5, 6 and 7; similar to Carlson and Ripley (1997) and Giannini et al. (2015).

$$NDVI = \frac{Band5(near\ infrared\ band) - Band4(red\ band)}{Band5(near\ infrared\ band) + Band4(red\ band)} \quad (4)$$

$$PV = \left(\frac{NDVI - NDVImin}{NDVImax - NDVI\ min}\right)^2 \quad (5)$$

$$Emissivity(e) = 0.004 \times PV + 0.986 \quad (6)$$

$$LST = \frac{BT}{1+\left(\frac{\lambda \times BT}{\rho}\right)\times \ln(e)} \quad (7)$$

Where λ is the central band wavelength of the thermal band (band 10) which ranges from 10.6 to 11.19 μm. In the present study, an average wavelength of 10.8 μm is applied. (ρ) is related to Boltzmann's constant (σ), Planck's constant (h), and speed of light (c) as follow:

$$\rho = \frac{h \times c}{\sigma\ (1.438 \times 10^{-2} m \cdot k)} \quad (8)$$

In addition, standard deviation was calculated for LST in all landfills to monitor the variations in different landfills as below (Altman & Bland, 2005):

$$\mathrm{SD} = \sqrt{\frac{\sum_{i=1}^{n}(LST_i - \overline{LST})}{n-1}} \quad (9)$$

Where, LST_i is land surface temperature for pixel i, $\overline{LST}$ is the average LST, and n is the number of pixels that cover the area in vicinity of landfills. Ultimately, coefficient of variations (CV) identified as equation 9 to show the relative spread of data compare to their average values.

$$CV = \frac{SD}{\overline{LST}} \quad (10)$$

Landsat imagery is also used for classification. Individual classes by Anderson (1976) are individually examined at the eight landfill sites. All classes are clustered using maximum likelihood estimation (MLE), and training iterations were run to minimize errors. MLE classification systems recognize each class by the average value of that specific class in each spectral band. A class is determined by a spectral signature considering the spread of the dataset in the relative spectrum. A normal distribution of data in each class is one of the assumptions for MLE classes. Ultimately, a membership matrix is embedded for the classification system where the probability of allocating each pixel to each specific class is clarified. Further details are provided by Myung (2003). Over 500 points in each landfill were used ground truth points and

were considered individually. The kappa coefficient of classification matrices for all landfills were greater than 0.80, which is sufficient for classifications similar to Jog and Dixit (2016).

The 'Majority 4 m' and 'boundary clean' filters are used to enhance the quality of the final classified image (Esri, 2020). The 'Majority 4 m' filter alternates pixels' values by considering the majority value that appears in the adjacent eight cells. Ultimately, this majority filter smooths the edgy (or 'salt and pepper') pattern of the final classified image. Moreover, the 'boundary clean' function filters borders between two classes to soften the overall pattern of classification by either expansion or shrinkage (Esri, 2020). A similar methodology is used in a previous study (Karimi et al. 2020). A total of six classes are considered in each buffer ring: forest, agricultural, rangeland, urban land, barren, and water.

Zonal statistics such as minimum, maximum, average, and standard deviation of LST and NDVI are calculated for each individual 30-meter buffer rings for all landfills, and the dominating classes are selected for further analysis. Results from Mahmood et al. (2019) and Shaker et al. (2010) suggested that higher LST may occur in regions of poor vegetative health (i.e. a lower NDVI), therefore the trends between LST and NDVI are explored to examine potential relationships at Canadian engineered landfills. Correlation analysis of LST and NDVI are investigated for each landfill to verify their potential correlation. The workflow of the present study is illustrated graphically in Supplementary Figure 2

3-Results and discussions

3-1-Land use classifications

Although all eight landfills are located in Canada and are subjected to similar landfill design philosophy and environmental regulations, the land use classification results show subtle differences among them (Figure 2). Forest land, agricultural land, and rangeland are most common at the landfill sites. It appears that the geospatial location of the landfill may impact the classification results. For instance, Western Canada's landfills, located in British Columbia (Hartland, Golden, Vancouver and Glenmore) are mostly in proximity to forest land, agricultural land, and rangeland. On the other hand, the Regina landfill, located in the southern prairies, is mostly covered by agricultural land and rangeland. For Eastern Canada's landfills, located in Ontario (Toronto, W12A and Durham), a mixture of all classes is present. The variations in land use in proximity to the eight landfills are expected given the climatic differences at each site, and a more open-ended design approach in Canadian landfill design standards and regulations (Richter et al. 2019).

The last column in Figure 2 shows the average classification results from the eight landfills. The combination of forest and agricultural land represents over 50% of the classified land. Since a significant part of landfill sites are made up of forest and agricultural lands, these two classes are selected and separately assessed.

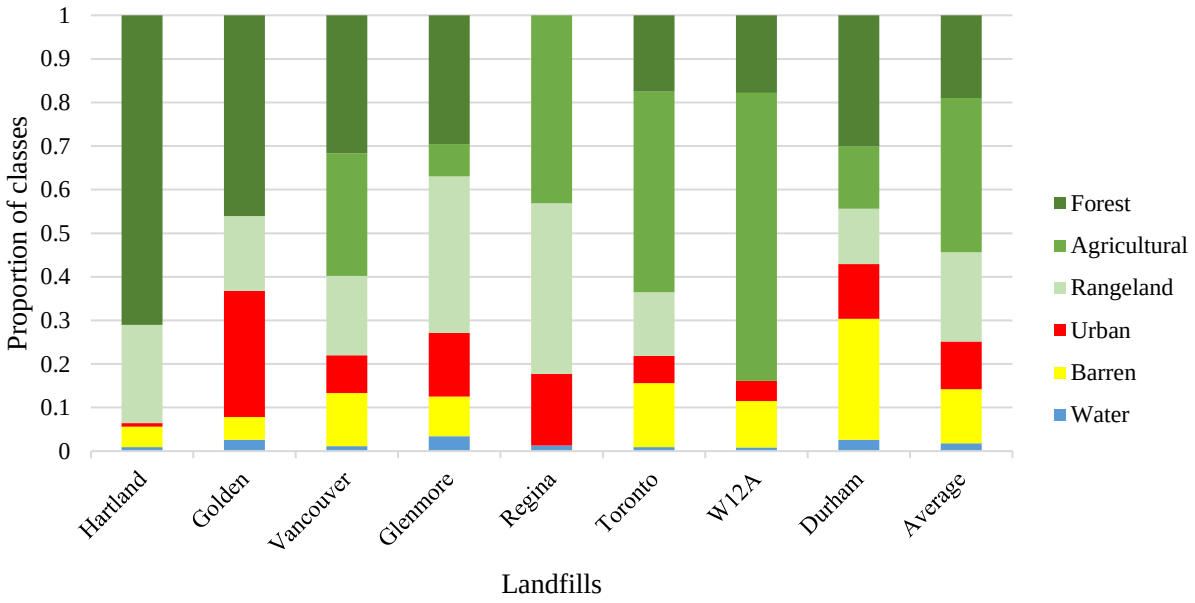

Figure 2 - LULC classes of the eight Canadian landfills

3-2-Land surface temperature

The mean temperature with respect to distance within forest land is shown in Figure 3. Regina does not have an identifiable forest class (Figure 2) and is thus ignored. In all seven landfill sites, the forest LST ranges from 18.3 °C to 29.5 °C. The coefficients of variation (CV) of LST range from 0.012 (W12A and Toronto) to 0.026 (Golden). The spread of LST appears narrower at landfill sites with less forest (Figure 2). Golden and Hartland, on the other hand, have the largest LST spread and are located in predominantly forested areas. Both landfills have relatively rounded footprint (Figure 1).

Due to the nature of the data, scattering of LST data is common, and regression analysis is used to identify trends. With the exception of Vancouver and Durham, linear regression shows a decreasing LST trend in the forest class within the first 1500 m of the landfill perimeter for five of the seven landfills. The positive slope of the trend at Vancouver ($m = +0.0005$, $R^2 = 0.17$) is more

obvious than at Durham (m = +0.0003, R^2 = 0.20). Peak LST is observed at the Vancouver landfill site around 810 m to 840 m. A closer look at the site reveals that the corresponding buffer rings are in proximity of a stretch of paved road south of the Vancouver landfill (Supplementary Figure 1c). It is hypothesized that the lack of forest land may have skewed the LST measurements, and that infrastructure should be accounted for in remote sensing studies near landfills. Regression analysis is used to investigate LST within forest classes in closer proximity to landfills. For distances within 300 m from the perimeter of the sites, all seven sites shown decreasing linear trendlines in the forest class. The Golden landfill has the flattest slope (m = -0.0015, R^2 = 0.64) within the 300 m, probably due to smaller footprint (64,486 m^2, as shown in Table 3). A relatively flat trendline is also observed at Durham, with a footprint of 59,233 m^2. On the other hand, the general shape of the landfill footprint appears insignificant to variations in LST, as Hartland, Durham, and Golden all have rounded footprints (Figure 1).

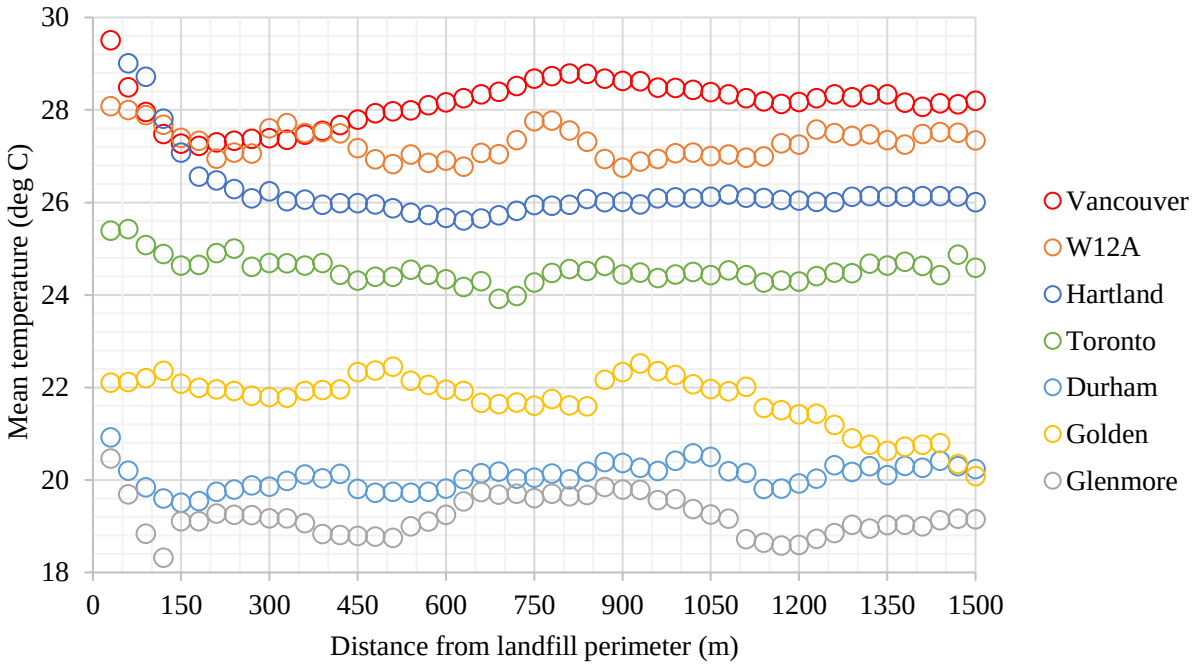

Figure 3 - Distance dependent LST for forest class

Table 4 summarizes the estimated size of the bio-thermal zone with respect to the forest class. A bio-thermal zone is an area that has elevated surface temperature due to the siting and operation of an engineered landfill. In this study, bio-thermal zone size is defined by the minimum distance from the landfill perimeter to an observed increase in mean LST. With the exceptions of Golden and Toronto landfills, the estimated bio-thermal zones range from 150 to 300 m from the perimeter. The estimated bio-thermal zone at Golden (30 m) may be less reliable due to a lack of obvious decreasing trend (Figure 2). Moreover, the estimated bio-thermal zone size at Toronto (60 m) is determined by a slightly higher mean LST of 25.4 °C at 60 m (Figure 2). If this single data point is ignored, then the estimated size for Toronto landfill is 180 m.

Table 4 – Estimated size of the bio-thermal zone with respect to forest and agricultural classes

	Forest land	**Agricultural land**
	Distance from perimeter to observe an increase in mean temperature (m)	Distance from perimeter to observe an increase in mean temperature (m)
Golden	30	N/A
Glenmore	150	240
Durham	180	30
Toronto	60	270
Vancouver	210	270
W12A	240	90
Hartland	300	N/A
Regina	N/A	180
Mean	167.14	180.00
Standard Deviation	89.08	91.65
Coefficient of variation	0.53	0.51

The LST curves for agricultural land are shown in Figure 4. Only six landfills (W12A, Regina,

Vancouver, Durham, Glenmore, and Toronto) are shown since they all have observable agricultural land near the sites (Figure 2). Compared to forest land (Figure 3), the LST of agricultural land at the sites are about 1-2 °C higher, ranging from 21.3 °C to 29.7 °C (Figure 4). The CV of LST for agricultural land ranges from 0.014 (W12A) to 0.107 (Toronto). In other words, both the magnitude and the variability of LST are higher in agricultural land. It appears that forest land has higher buffering capacity and is less sensitive to the microclimate than agricultural land.

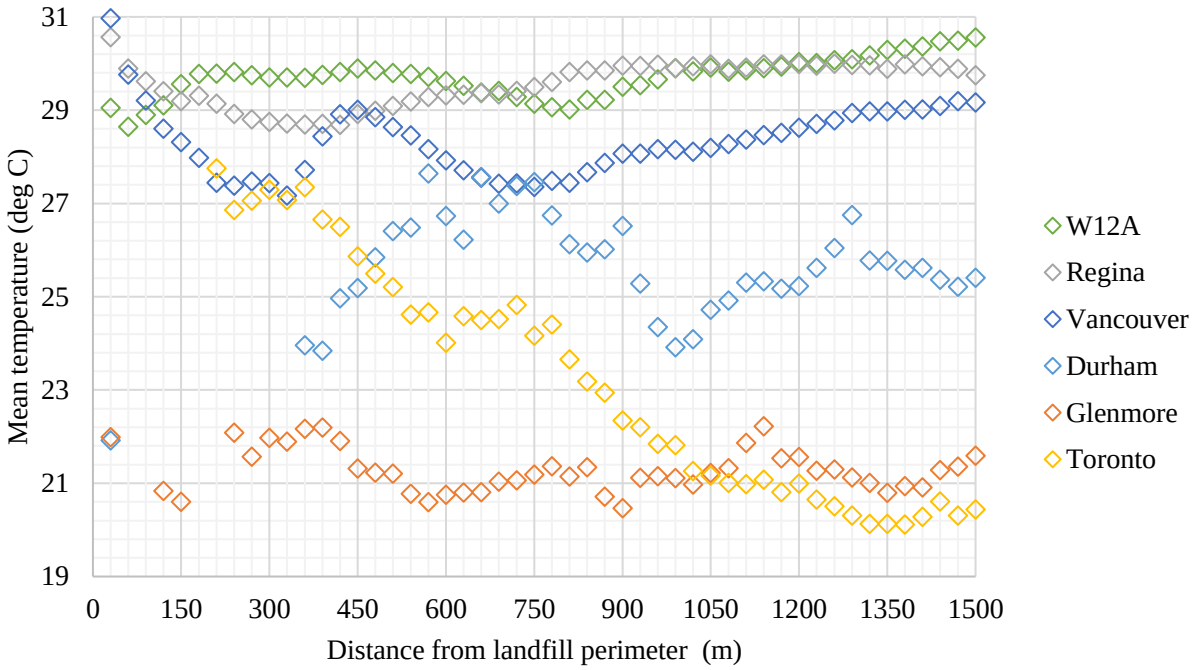

Figure 4 - Distance dependent LST for agricultural classes

As shown in Figure 4, the LST with respect to distance is more erratic in agricultural land than in forest land. Given that agricultural land, on average, is almost double the percentage compared to forest land (Figure 2), one would expect a more gradual change of LST. It is believed that LST of agricultural land is strongly influenced by farming practices, including cropland geospatial distribution, crop type, planting density, irrigation scheme, and the seed, nurture and harvest schedule. Obvious decreasing trends are generally not observed in Figure 4. Linear regression

shows decreasing LST trends within the first 1,500 m of the landfill perimeter for only two out of six landfills: Toronto (m = -0.0064, R^2 = 0.95) and to a lesser degree, Glenmore (m = -0.0002, R^2 = 0.04).

Toronto has a consistent decreasing trend unlike others, representing a 7 °C drop at 1,500 m from the landfill perimeter. Landfill specifications such as landfill perimeter, shape and area, and disposal rates (shown in Table 3) have failed to explain the consistent decreasing trend of the LST for agricultural class at Toronto. Higher fluctuations are also observed at the Durham and Glenmore landfills, probably due to the absence of agricultural land, especially within 360 m from the landfill perimeter.

The estimated size of bio-thermal zone with respect to agricultural land is shown in Table 4, and ranges from 30 m to 270 m. Although the mean and CV of the resulting sizes from the two classes are similar, the size of the bio-thermal zone appears sensitive to the selected LULC class. The result suggests that bio-thermal zone should be reported together with the LULC class for meaningful interpretation. Among the sites, the estimated sizes of bio-thermal zone are the most consistent at Vancouver landfill (210 m vs. 270 m), probably due to an equal spread of forest and agricultural land (Figure 2). Given the nature of the data, one standard deviation is adopted to report the size of bio-thermal zone. The approximate bio-thermal zones for forest class and agricultural classes are thus about 170 ± 90 m and 180 ± 90 m from the perimeter of landfill, respectively.

3.3 Correlations between LST and NDVI

In this study, NDVI is used as an indicator to assess vegetation health near the selected landfill sites. Correlational analysis between NDVI and LST for both forest land and agricultural land

367 within 1,500 m of the landfill perimeter are conducted. For the forest class, NDVI was negatively
368 correlated (-0.30 to -0.69) with LST at 6 out of 7 landfills, with the exception of the Glenmore
369 landfill (Table 3). It is not clear why NDVI is positively correlated to LST with a coefficient of +
370 0.35 at Glenmore landfill, as one would expect a denser vegetative cover would lower the LST
371 (Waseem and Khayyam 2019). For example, Dong et al. (2020) found that even small area of
372 green roofs in urban area has observable cooling effect at the city scale. It is found that the NDVI
373 within the forest class at Glenmore has the lowest mean NDVI of 0.246, and the predominance of
374 non-vegetated areas or bare land may have skewed the results.
375 Stronger relationships are observed in the agricultural class with coefficients from -0.44 to -
376 0.97 (Table 3). The negative coefficients suggest that elevated LST in close proximity to landfills
377 is associated poorer vegetative health. The differences in correlation coefficients between NDVI
378 and LST again highlight the use of LULC class for bio-thermal zone identification. Agricultural
379 lands appear more sensitive than forest land and can easily be deteriorated by temperature
380 fluctuations. The results generally support the use of NDVI as a complementary indicator to
381 monitor bio-thermal effects of landfills.
382

383 ## 3.4 Rate of change of LST and NDVI

384 The averaged coefficient of variation of the LST and NDVI using all classes at each 30-m
385 buffer ring in all sites are plotted with respect to distance (Figure 5) to study the trend and
386 variability of the indictors. The variabilities of both indicators increase with distance, but at
387 different rates. The slope of the linear regression line for NDVI (m = +0.101, R^2 = 0.62) is about
388 double that of the LST (m = +0.050, R^2 = 0.80). NDVI has considerably larger spread, and is less
389 consistent than LST. CV of LST are mostly around 4.0 within the bio-thermal zone (0 - 270 m),

or mostly under 6.0 at a distance of 1,500 m. CV of NDVI, on the other hand, ranges from 9.8 to 12.5 within the bio-thermal zone, and up to 18.5 if the entire 1,500 m range is considered. Results suggested that LST data is more precise and may be more appropriate with respect to the identification of bio-thermal zone near landfills.

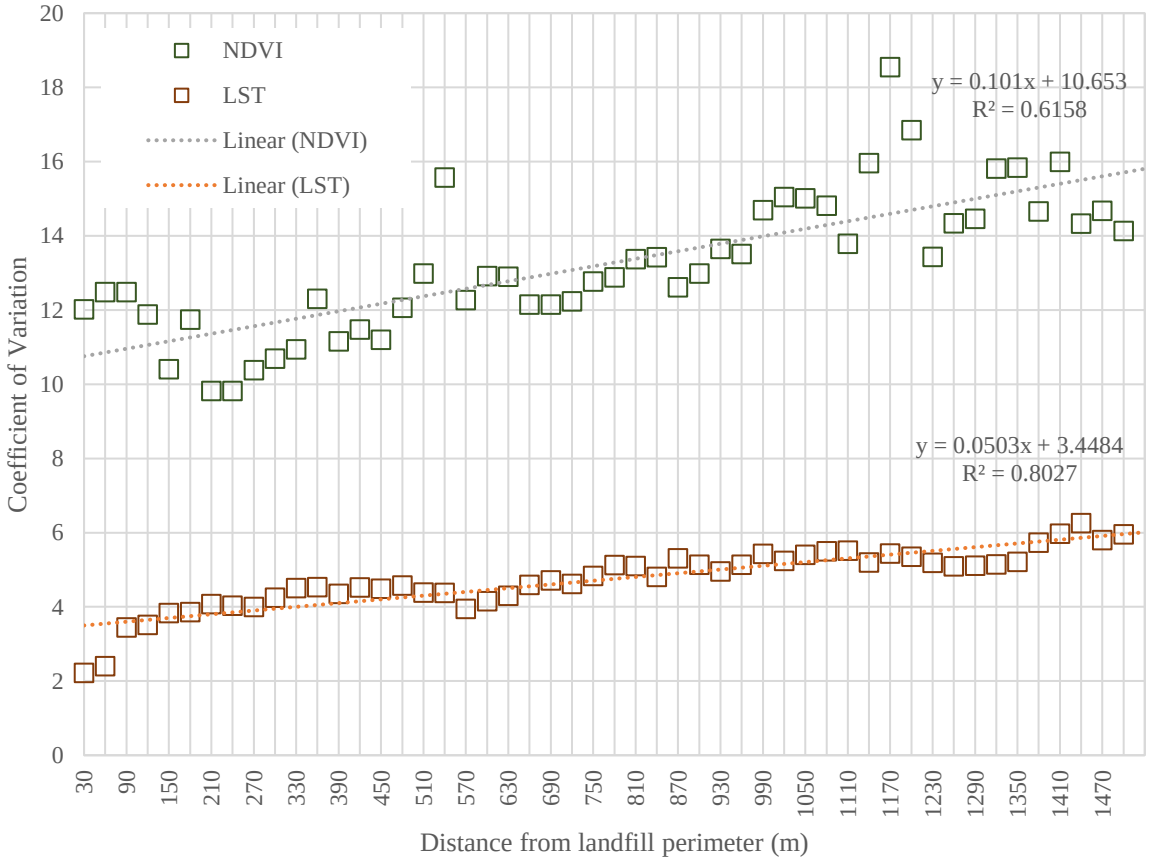

Figure 5 - Coefficient of variation for LST and NDVI within each 30 m ring

The average LST of the sites with respect to six LULC classes is shown in Figure 6. A subtle but observable difference in LST is observed among LULC classes. Forest lands have the lowest

403 average temperature of 23.9 °C, followed by water with 24.3 °C. Major water bodies typically
404 have lower LST than other LULC classes but it is not the case in the present study. Water bodies
405 in close proximity to the landfills (<1,500 m) are likely small depressions with impeded drainage
406 instead of a large surface water bodies due to the siting requirements of Canadian landfills. This
407 explanation is consistent with the finding that water bodies in this study are small and represent
408 less than 2% of the total area (Figure 2).

409 Intensified vegetation associated with the forest class acts as a heat sink and helps undermine
410 temperature rise. Agricultural land has slightly higher LST than rangeland, probably due to the
411 elevated crop density and optimized irrigation scheme in modern agricultural practices. The urban
412 class (27.1 °C) and barren class (27.4 °C) show the highest average temperature, both of which are
413 likely to have small vegetation cover. Geometric shape makes no observable difference in LST,
414 however, larger landfills appear to have higher LST, at least from the eight Canadian engineered
415 landfill data.

416

417

418

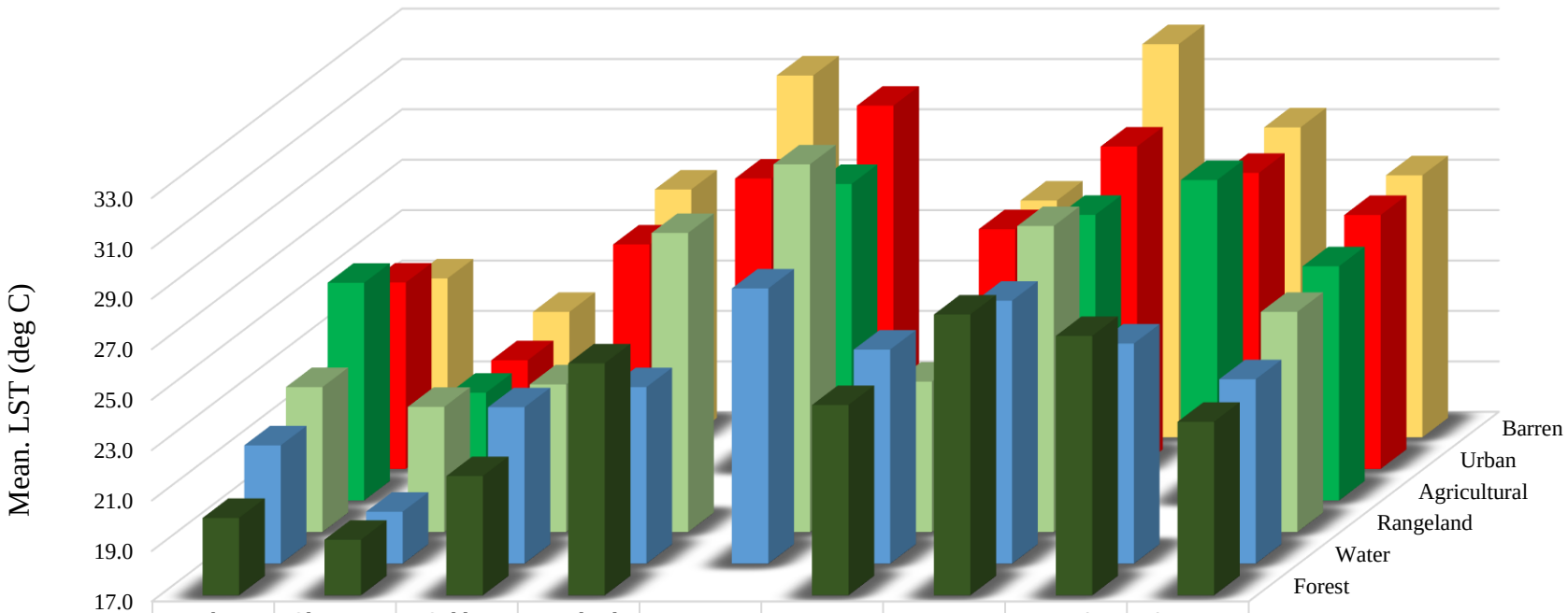

	Durham	Glenmore	Golden	Hartland	Regina	Toronto	Vancouver	W12A	Average
Forest	20.1	19.2	21.7	26.2		24.5	28.1	27.3	23.9
Water	21.7	19.1	23.2	24.0	27.9	25.5	27.4	25.7	24.3
Rangeland	22.7	22.0	22.9	28.9	31.6	23.0	29.1		25.7
Agricultural	25.6	21.3			29.6	23.2	28.3	29.7	26.3
Urban	24.4	21.3	25.9	28.5	31.4	26.5	29.8	28.7	27.1
Barren	23.3	22.0	26.8	31.4		26.4	32.6	29.3	27.4

Landfills

Figure 6 - Average land surface temperature at each landfill with respect to six LULC classes

3.5 Limitations and recommendations

Although Landsat satellite images are widely available and accessible, many of the images contain cloud cover or haziness over the target sites, limiting their usefulness as inputs. This is particularly challenging in the present study, as all the Landsat scenes selected were from a short period (June to August) for multiple landfills located across Canada to facilitate comparison. We found that LST near landfills is sensitive to LULC class, and as such, caution should be used when comparing results from different time periods and regions. Even under an ideal situation, remote sensing techniques are only capable of capturing the condition of the Earth's surface, and it should not be used to replace conventional in-situ monitoring of waste deposal sites. In addition, migration of leachate and landfill gases could impact LST and vegetation health near disposal sites.

Since most bio-thermal activities in landfills start within a couple of years of waste placement, covered/capped and active areas may be determining factors for detection of the bio-thermal zone. The shadow of the waste mountain, and site elevation and may also contribute to LST (Khandelwal et al. 2018). The research is on-going and the results related to topographical feature and cover design on LST will be reported in a future paper. Analysis with a more comprehensive classification system (type of trees, crops, soil, etc) can be included to better quantify the impact of waste disposal site. A temporal analysis is also recommended, where Landsat images from different years are considered to assess the long-term impact. Education on waste minimization and progressive reduction of landfilling are some of the key components in a circular economy. The reliance on land disposal as the primary waste treatment method is not sustainable, and more work on refinement of the waste hierarchy is recommended.

4.0 Conclusion

Urbanization and lack of suitable landfill sites in cities have generated a need for more stringent knowledge of land information for sustainable natural resource management and better wildlife habitat protection. There is a lack of understanding on the extent and severity of the bio-thermal zone of engineered landfills. In this study, a total of eight Canadian landfills with various size and shape and climatic conditions are selected to quantify the spatial extent of the bio-thermal zone using LST and NDVI. Results are specifically discussed with respect to six selected LULC classes. Quantification of the spatial extent of bio-thermal zone is important and may help to improve current landfill design regulations.

It was found that forest land and agricultural land are most common near the landfills in Canada. Together, these classes represented more than half of the total study area. For forest land, LST ranged from 18.3 °C to 29.5 °C within 1,500 m of the sites during the study period, with CV of 0.012 to 0.026. Linear regression shows a decreasing LST trend within the first 1,500 m of the landfill perimeter for five out of seven landfills. For distance within 300 m from the perimeter of the sites, all seven sites showed decreasing linear trendlines. The LST of agricultural land ranged from 21.3 °C to 29.7 °C, with a CV of 0.014 - 0.107. The decreasing trend between LST and distance for agricultural land are generally not observed. Both the magnitude and the variability of LST are higher in agricultural land. It appears that agricultural land has lower buffering capacity and is more sensitive to the microclimate than forest land.

The bio-thermal zone size is found sensitive to the selected LULC class, and the approximate bio-thermal zones for forest class and agricultural classes are about 170 ± 90 m and 180 ± 90 m from the perimeter of landfill, respectively. The result suggests that bio-thermal zone should be reported together with the LULC class for meaningful interpretation.

For the forest class, NDVI was negatively correlated (-0.30 to -0.69) with LST at six out of seven Canadian landfills. Stronger relationships are found in the agricultural class with coefficients from -0.44 to -0.97. NDVI has considerably larger spread and is less consistent than LST. CV of LST is mostly under 6.0 at a distance of 1,500m, whereas CV of NDVI can be up to 18.5. The results generally support the use of NDVI as a complementary indicator to monitor bio-thermal effects of the landfills. Overall, LST data may be more appropriate with respect to the identification of landfill bio-thermal zone.

A subtle difference in LST is observed among six LULC classes. Forest lands have the lowest average temperature of 23.9 °C, followed by water with 24.3 °C. The urban class (27.1 °C) and barren class (27.4 °C) show the highest average temperature. Geometric shape makes no observable difference in LST in this study; however, larger landfill footprint appears to have a higher LST. It is believed the proposed analytical framework is also applicable to engineered landfills located in other countries.

Acknowledgements: The research reported in this paper was supported by a grant from the Natural Sciences and Engineering Research Council of Canada (RGPIN-2019-06154) to the corresponding author (K.T.W. Ng), using computing equipment funded by FEROF at the University of Regina. The authors are grateful for their support. The views expressed herein are those of the writers and not necessarily those of our research and funding partners.

References

Ali, S.M., Pervaiz, A., Afzal, B., Hamid, N., & Yasmin, A. (2014). Open dumping of municipal solid waste and its hazardous impacts on soil and vegetation diversity at waste dumping sites of Islamabad city. Journal of King Saud University-Science, 26, 59-65

Altman, D. G., & Bland, J. M. (2005). Standard deviations and standard errors. Bmj, 331(7521), 903.

Anderson, J.R. (1976). A land use and land cover classification system for use with remote sensor data. US Government Printing Office

Annual monitoring Report (2017), Durham Waste Disposal Site, Municipality of West Grey, MOECC

494 Azeez, J.O., Hassan, O.A., & Egunjobi, P.O. (2011). Soil Contamination at Dumpsites: Implication of Soil Heavy
495 Metals Distribution in Municipal Solid Waste Disposal System: A Case Study of Abeokuta, Southwestern
496 Nigeria. Soil and Sediment Contamination: An International Journal, 20, 370-386

497 Barsi, J.A., Barker, J.L., & Schott, J.R. (2003). An atmospheric correction parameter calculator for a single thermal
498 band earth-sensing instrument. In, IGARSS 2003. 2003 IEEE International Geoscience and Remote Sensing
499 Symposium. Proceedings (IEEE Cat. No. 03CH37477) (pp. 3014-3016): IEEE

500 Barsi, J.A., Schott, J.R., Palluconi, F.D., & Hook, S.J. (2005). Validation of a web-based atmospheric correction tool
501 for single thermal band instruments. In, Earth Observing Systems X (p. 58820E): International Society for
502 Optics and Photonics

503 Basso, B., Cammarano, D., & De Vita, P. (2004). Remotely sensed vegetation indices: Theory and applications for
504 crop management. Rivista Italiana di Agrometeorologia, 1, 36-53

505 Bellezoni, R.A., Iwai, C.K., Elis, V.R., da Silva Paganini, W., & Hamada, J. (2014). Small-scale landfills: impacts on
506 groundwater and soil. Environmental earth sciences, 71, 2429-2439

507 Biotto, G., Silvestri, S., Gobbo, L., Furlan, E., Valenti, S., & Rosselli, R. (2009). GIS, multi-criteria and multi-factor
508 spatial analysis for the probability assessment of the existence of illegal landfills. International Journal of
509 Geographical Information Science, 23, 1233-1244

510 Bruce, N., Ng, K. T. W., and Vu, H. L. (2018) "Use of Seasonal Parameters and their Effects on FOD Landfill Gas
511 Modeling". Environmental Monitoring and Assessment, 190:291. https://doi.org/10.1007/s10661-018-6663-
512 x

513 Cai, B.-F., Jian-Guo, L., Qing-Xian, G., Xiao-Qin, N., Dong, C., Lan-Cui, L., Ying, Z., & Zhan-Sheng, Z. (2014).
514 Estimation of methane emissions from municipal solid waste landfills in China based on point emission
515 sources. Advances in climate change research, 5, 81-91

516 Carlson, T.N., & Ripley, D.A. (1997). On the relation between NDVI, fractional vegetation cover, and leaf area index.
517 Remote sensing of Environment, 62, 241-252

518 Chander, G., & Markham, B. (2003). Revised Landsat-5 TM radiometric calibration procedures and postcalibration
519 dynamic ranges. IEEE Transactions on geoscience and remote sensing, 41, 2674-2677

520 Chowdhury, A., Vu, H. L., Ng, K. T. W., Richter, A. and Bruce, N. (2017) "An Investigation on Ontario's Non-
521 hazardous Municipal Solid Waste Diversion using Trend Analysis". Canadian Journal of Civil Engineering,
522 44(11), 861–870. https://dx.doi.org/10.1139/cjce-2017-0168

523 City of Regina (2009) Fleet Street Solid Waste Disposal and Recovery Facility Expansion Project, prepared for: City
524 of Regina Public works division. AMEC Earth and Environmental, Regina, Saskatchewan, September.

525 City of Toronto, 2017 Annual Progress Report, Green Lane landfill, WSP, Canada

526 Cristóbal, J., Jiménez-Muñoz, J. C., Prakash, A., Mattar, C., Skoković, D., & Sobrino, J. A. (2018). An improved
527 single-channel method to retrieve land surface temperature from the Landsat-8 thermal band. Remote
528 Sensing, 10(3), 431.

529 Dong, J., Lin, M., Zuo, J., Lin, T., Liu, J., Sun, C., Luo, J. (2020) Quantitative study on the cooling effect of green
530 roofs in a high-density urban Area—A case study of Xiamen, China. Journal of Cleaner Production, 255,
531 120152. https://doi.org/10.1016/j.jclepro.2020.120152

532 Esri, 2020. Smoothing zone edges with boundary clean and majority filter retrieved from
533 http://desktop.arcgis.com/en/arcmap/10.3/tools/spatial-analyst toolbox/smoothing-zone-edges-with-
534 boundary-clean-and-majority-filter.htm, 2020.01.14

535 Garkowski, J., and Hostovsky, C. (2011) Policy versus practice in Municipal Solid Waste Diversion: the Role of the
536 waste crisis in Ontario waste planning. Canadian Journal of Urban Research, 20(1), 81-102.

537 Giannini, M., Belfiore, O., Parente, C., & Santamaria, R. (2015). Land Surface Temperature from Landsat 5 TM
538 images: comparison of different methods using airborne thermal data. Journal of Engineering Science &
539 Technology Review, 8

540 Glenmore Landfill Annual Report Operational Certificate (2017), MR 12218 EMS reference # E104956, city of
541 Kelowna

542 Hanson, J.L., Yeşiller, N., & Oettle, N.K. (2009). Spatial and temporal temperature distributions in municipal solid

waste landfills. Journal of Environmental Engineering, 136, 804-814

Hao, Z., Sun, M., Ducoste, J., Benson, C., Luettich, S., Castaldi, M., Barlaz, M. 2017. Heat Generation and Accumulation in Municipal Solid Waste Landfills. Environ. Sci. Technol. 51, 21, 12434–12442. https://doi.org/10.1021/acs.est.7b01844

Hartland Landfill (2016) Annual Report, Operating & Environmental Monitoring, Prepared by Korene Torney, Geo-Environmental Programs, Environmental Protection

Iacoboaea, C., & Petrescu, F. (2013). Landfill monitoring using remote sensing: a case study of Glina, Romania. Waste Management & Research, 31, 1075-1080

Karimi, H., Amiri, S., Huang, J., & Karimi, A. (2019). Integrating GIS and multi-criteria decision analysis for landfill site selection, case study: Javanrood County in Iran. International Journal of Environmental Science and Technology, 16, 7305-7318

Karimi, N., Richter, A., and Ng, K. T. W. (2020) "Siting and ranking municipal landfill sites in regional scale using nighttime satellite imagery". Journal of Environmental Management, 256, 109942. https://doi.org/10.1016/j.jenvman.2019.109942

Khandelwal, S., Goyal, R., Kaul, N., Mathew, A. (2018) "Assessment of land surface temperature variation due to change in elevation of area surrounding Jaipur, India" The Egyptian Journal of Remote Sensing and Space Science, 21(1), 87-94. https://doi.org/10.1016/j.ejrs.2017.01.005

Koerner, G.R., & Koerner, R.M. (2006). Long-term temperature monitoring of geomembranes at dry and wet landfills. Geotextiles and Geomembranes, 24, 72-77

LANDSAT 8 (L8) DATA USERS HANDBOOK, Department of interior US. Geological Survey. 2018. Acquired from https://www.usgs.gov/media/files/landsat-8-data-users-handbook on 2019.10.20

Li, Y., Zhao, M., Motesharrei, S., Mu, Q., Kalnay, E., & Li, S. (2015). Local cooling and warming effects of forests based on satellite observations. Nature Communications, 6, 6603

Mahmood, K., Batool, A., Faizi, F., Chaudhry, M.N., Ul-Haq, Z., Rana, A.D., & Tariq, S. (2017). Bio-thermal effects of open dumps on surroundings detected by remote sensing—Influence of geographical conditions. Ecological Indicators, 82, 131-142

Mahmood, K., Batool, S.A., & Chaudhry, M.N. (2016). Studying bio-thermal effects at and around MSW dumps using Satellite Remote Sensing and GIS. Waste Management, 55, 118-128

Mahmood, K., Ul-Haq, Z., Faizi, F., & Batol, S.A. (2019). A comparison of satellite-based indices for hazard assessment of MSW open dumps using spatial analysis. Waste Management & Research, 37, 219-236

Myung, I. J. (2003). Tutorial on maximum likelihood estimation. Journal of mathematical Psychology, 47(1), 90-100.

Nasa. 2019. Atmospheric correction parameter calculator retrieved from https://atmcorr.gsfc.nasa.gov/ by 2020/04/01

Nikam, B. R., Ibragimov, F., Chouksey, A., Garg, V., & Aggarwal, S. P. (2016, 2016/08/12). Retrieval of land surface temperature from Landsat 8 TIRS for the command area of Mula irrigation project. Environmental earth sciences, 75(16), 1169. https://doi.org/10.1007/s12665-016-5952-3

Pan, C., Bolingbroke, D., Ng, K. T. W., Richter, A., and Vu, H. L. (2019a) "The Use of Waste Diversion Indices on the Analysis of Canadian Waste Management Models". Journal of Material Cycles and Waste Management, 21(3), 478-487. https://doi.org/10.1007/s10163-018-0809-3

Pan, C., Ng, K. T. W., and Richter, A. (2019b) "An Integrated Multivariate Statistical Approach for the Evaluation of Spatial Variations in Groundwater Quality near an Unlined Landfill". Environmental Science and Pollution Research, 26(6), 5724-5737. https://doi.org/10.1007/s11356-018-3967-x

Phil-Eze, P. (2010). Variability of soil properties related to vegetation cover in a tropical rainforest landscape. Journal of Geography and Regional planning, 3, 177-184

Ramachandra, T.V., Bharath, S., Gupta, N. (2018) Modelling landscape dynamics with LST in protected areas of Western Ghats, Karnataka. Journal of Environmental Management, 206, 1253-1262. https://doi.org/10.1016/j.jenvman.2017.08.001

Richter, A., Ng, K. T. W., and Fallah, B. (2019) "Bibliometric and Text Mining Approaches to Evaluate Landfill Design Standards". Scientometrics, 118(3), 1027-1049. https://doi.org/10.1007/s11192-019-03011-4

Richter, A., Ng, K. T. W., and Pan, C. (2018) "Effects of Percent Operating Expenditure on Canadian Non-hazardous

592 Waste Diversion". Sustainable Cities and Society, 38, 420-428. https://dx.doi.org/10.1016/j.scs.2018.01.026
593 Shaker, A., Faisal, K., El-Ashmawy, N., & Yan, W. (2010). Effectiveness of using remote sensing techniques in
594 monitoring landfill sites using multi-temporal Landsat satellite data. Al-Azhar University Engineering
595 Journal, 5, 542-551
596 Sharma, A., Gupta, A.K., & Ganguly, R. (2018). Impact of open dumping of municipal solid waste on soil properties
597 in mountainous region. Journal of Rock Mechanics and Geotechnical Engineering, 10, 725-739
598 Silleos, N.G., Alexandridis, T.K., Gitas, I.Z., & Perakis, K. (2006). Vegetation indices: advances made in biomass
599 estimation and vegetation monitoring in the last 30 years. Geocarto International, 21, 21-28
600 S. Jog and M. Dixit, "Supervised classification of satellite images," 2016 Conference on Advances in Signal
601 Processing (CASP), Pune, 2016, pp. 93-98, doi: 10.1109/CASP.2016.7746144.
602 Sobrino, J.A., Jiménez-Muñoz, J.C., & Paolini, L. (2004). Land surface temperature retrieval from LANDSAT TM 5.
603 Remote sensing of Environment, 90, 434-440
604 Golden (2017) Annual Operations and Monitoring Report, Golden Refuse Disposal Site MR-17006, 2017, Prepared
605 by: Ben Van Nostrand, Environmental Health Services, Columbia Shuswap Regional District Operations
606 Management
607 Statistics Canada, 2019. Canada at a glance, Environmental edition. Waste. Retrieved from
608 https://www150.statcan.gc.ca/n1/pub/12-581-x/2017001/sec-5-eng.htm on 2020.01.22
609 IPCC, 2019. Waste management, The Intergovernmental Panel on Climate Change. Retrieved from
610 https://www.ipcc.ch/site/assets/uploads/2018/02/ar4-wg3-chapter10-1.pdf on 2019.10.24
611 Ullah, S., Ahmad, K., Sajjad, R.U., Abbasi, A.M., Nazeer, A., Tahir, A.A. (2019) Analysis and simulation of land
612 cover changes and their impacts on land surface temperature in a lower Himalayan region. Journal of
613 Environmental Management, 245, 348-357. https://doi.org/10.1016/j.jenvman.2019.05.063
614 USGS. (2020). Landsat 8 instruments and details, retrieved from https://www.usgs.gov/land-
615 resources/nli/landsat/landsat-8?qt-science_support_page_related_con=0#qt-
616 science_support_page_related_con by 2020/07/26
617 USGS. (2018). Landsat level1 image (L1GT) acquired from Global Visualization Viewer (GloVis),
618 https://glovis.usgs.gov/ on 2018.12.15
619 Vancouver Landfill (2017) Annual Report, BC Ministry of Environment and Climate Change Strategy. Prepared by:
620 City of Vancouver Engineering Services Transfer and Landfill Operations
621 W12A Annual Report (2017) Waste Generation Projections & Landfill Capacity Assessment Prepared by City of
622 London, Ontario
623 Waseem, S. and Khayyam, U. (2019) Loss of vegetative cover and increased land surface temperature: A case study
624 of Islamabad, Pakistan. Journal of Cleaner Production, 234, 972-983.
625 https://doi.org/10.1016/j.jclepro.2019.06.228
626 Xu, Y., Xue, X., Dong, L., Nai, C., Liu, Y., & Huang, Q. (2018). Long-term dynamics of leachate production, leakage
627 from hazardous waste landfill sites and the impact on groundwater quality and human health. Waste
628 Management, 82, 156-166
629 Yan, W.Y., Mahendrarajah, P., Shaker, A., Faisal, K., Luong, R., & Al-Ahmad, M. (2014). Analysis of multi-temporal
630 Landsat satellite images for monitoring land surface temperature of municipal solid waste disposal sites.
631 Environmental monitoring and assessment, 186, 8161-8173. DOI 10.1007/s10661-014-3995-z
632 Yang, C., Yan, F., Zhang, S. (2020) Comparison of land surface and air temperatures for quantifying summer and
633 winter urban heat island in a snow climate city. Journal of Environmental Management, 265, 110563.
634 https://doi.org/10.1016/j.jenvman.2020.110563
635 Yu, X., Guo, X., & Wu, Z. (2014). Land surface temperature retrieval from Landsat 8 TIRS—Comparison between
636 radiative transfer equation-based method, split window algorithm and single channel method. Remote
637 Sensing, 6(10), 9829-9852.
638

639

640

641

Supplementary Materials

List of Supplementary Figures

- Supplementary Figure 1 - Vancouver landfill. (a) Layout of Vancouver landfill including active, capped and future phases (Source: Vancouver, 2017), (b) digitizing the actual boundaries of landfill using Arc-GIS10.5 software, (c) Construction of multiple ring buffer zone with 30-meter increments around the landfill for up to 1500 meters
- Supplementary Figure 2 - Workflow of the present study

a

b

c

Supplementary Figure 1 - Vancouver landfill. (a) Layout of Vancouver landfill including active, capped and future phases (Source: Vancouver, 2017), (b) digitizing the actual boundaries of landfill using Arc-GIS10.5 software, (c) Construction of multiple ring buffer zone with 30-meter increments around the landfill for up to 1500 meters

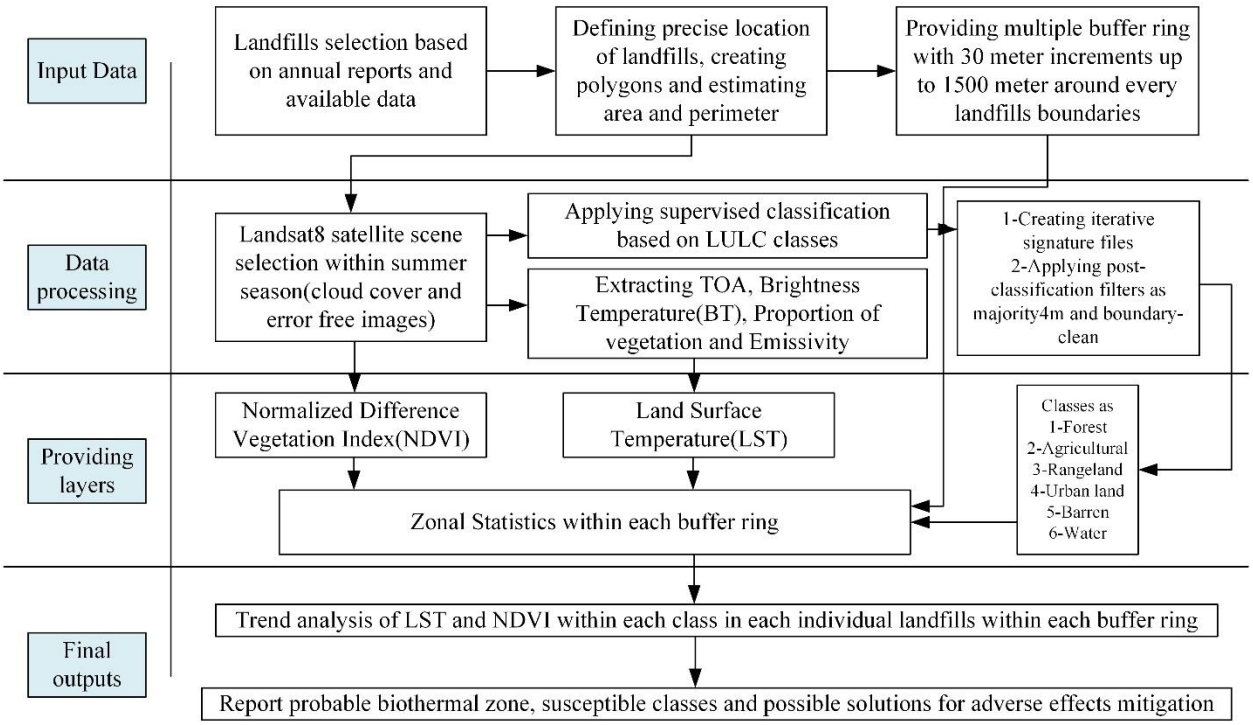

661

662 Supplementary Figure 2 - Workflow of the present study

663